Journal of Traffic and Transportation Engineering 7 (2019) 264-281
doi: 10.17265/2328-2142/2019.06.003

Design and Numerical Investigation to Predict the Flow Pattern of Non-axisymmetric Convergent Nozzle: A Component of Turboexpander

Manoj Kumar, Rasmikanti Biswal, Suraj Kumar Behera, and Ranjit Kumar Sahoo
Department of Mechanical Engineering, NIT, Rourkela, Odisha 769008, India

Abstract: Current work proposes a novel design methodology using curve-fitting approach for a non-axisymmetric airfoil convergent nozzle used in small-sized cryogenic turboexpander. The curves used for designing the nozzle are based on a combination of fifth and third order curve at upper and lower surface respectively. Four different turbulence model such as k-ε, SST, BSL and SSG Reynolds stress turbulence model is used to visualize and compare the fluid flow characteristics and thermal behaviors at various cross-sections. It is interesting to observe that the Mach number obtained at the outlet of the nozzle is highest and temperature drop is maximum for SSG model under similar boundary conditions. It is also observed that the designed nozzle with curve fitting approach is appropriate for impulse type turbine with a small amount of reaction. The key feature of this implementation is to obtain subsonic velocity at the nozzle exit and reduce the irreversible losses through the nozzle, which can affect the performance of a turboexpander.

Key words: Fluid flow pattern, non-axisymmetric nozzle, air, CFD, turboexpander.

Nomenclature

RANS	Reynold's averaged Navier-Stokes
TVD	Total variation diminishing
NVD	Normalized variable diagram
TKE	Turbulent kinetic energy
LES	Large eddy simulation
CFVN	Critical flow venturi nozzles
CFD	Computational fluid dynamics
DSMC	Direct simulation Monte Carlo
WALE	Wall-adapting local eddy-viscosity
WMLES	Algebric wall-modeled LES
SST	Shear-stress tensor
SSG	Speziale Sarkar and Gatski
BSL	Baseline

1. Introduction

The design of an efficient nozzle plays an important role in a turboexpander unit for the liquefaction of various cryogenic gases. The increasing requirements for efficient gas liquefaction plants demand the efficient cryogenic components, which are used in a turboexpander such as a nozzle, expansion turbine, brake compressor, diffuser etc. In this framework, researchers are interested to design an efficient and optimized nozzle profile, which is desirable to minimize the losses and compact shape of a turboexpander. Cryogenic fluids like liquid helium, nitrogen, oxygen, hydrogen etc. are used due to its variety of applications in the fields such as rocket propulsion and aerospace appliances, superconducting equipment, industrial applications etc. The advent of modern superconductors that will achieve superconductivity at or above liquid nitrogen temperature will increase the importance of liquid nitrogen as a cryogenic refrigerant [1].

Dadone and Grossman [2] suggested the design optimization methodology for inviscid fluid flow problems and its suitability for two and three-dimensional diffuser, airfoils nozzles and supersonic blunt bodies in the subsonic, supersonic

Corresponding author: Manoj Kumar, Ph.D., research fields: turboexpander, turbulent jet, phase change materials, heat exchanger. E-mail: manojbeg526@gmail.com.

and transonic flow. Scalabrim and Azevedo [3] discussed the impact of adaptive refinement technique on the quality of the solution for the transonic convergent-divergent nozzle, convergent nozzle and airfoil with a supersonic entrance using compressible flow equations. Tsui and Wu [4] described the pressure-based method to solve the incompressible and compressible flows past an airfoil and through the convergent-divergent and double throat nozzle using high-resolution TVD and NVD schemes. Horisawa et al. [5] validated the experimental results with numerical simulation for internal flow behavior of a rectangular micro-single-nozzle and multi-nozzle-array using DSMC method and optimized its geometry to achieve the increased propulsive efficiency.

The computational work to visualize the effect of nozzle pressure ratio on flow structure, shock-induced boundary layer separation inside a non-axisymmetric supersonic convergent-divergent nozzle was performed by Hasan [6]. Mousavi and Roohi [7] investigated the shock train in a three-dimensional convergent-divergent nozzle for compressible and turbulent fluid flow using Reynolds stress turbulence model (RSM) which is validated with the experimental data. Lavante et al. [8] investigated the flow behavior, shock structure and choking phenomenon in CFVN for exit pressure ratio vary in between 0.2 and 0.8 and at different Reynolds number (Laminar or turbulent) using self-developed Navier-Stokes solver ACHIEVE program and commercial code CD-adapco Star CCM+. Pengfei et al. [9] developed half-flexible single jack nozzle for supersonic free jet used in wind tunnel to achieve better aerodynamic performance, mechanical property, and continuous Mach number regulation. Chung et al. [10] used naphthalene sublimation method to investigate the flow field behavior, vortex formation and heat transfer near the nozzle end wall using CFD simulations and experiments. The work is carried on to investigate the wall pressure, flow separation, shock wave propagation and boundary layer transient flows through 3-D planar, supersonic convergent-divergent and Laval nozzle using different sub-grid models (WALE, WMLES, and Smagorinsky-Lilly) and proposed that WMLES provide best results using LES and validate it with experimental results [11-13]. The work was continued to predict the high pressure (70 MPa) hydrogen fluid flow behavior and its boundary layer pattern and concluded that fluid throat was generated due to viscous effects which acts as a convergent-divergent nozzle [14].

Detailed literature survey reveals that there are a plethora of works on convergent, convergent-divergent axisymmetric nozzles. Very little courtesy is given to the non-axisymmetric convergent nozzle. The first reported work on this topic is that of Turgut and Camci [15], who used non-axisymmetric end wall contouring method to minimize the secondary flow losses inside the turbine nozzle guide vane. The splines based on Fourier series at different locations are generated and connect it with streamwise B-Splines. Turbine stage was modeled as a series of nozzles by W.F. Fuls [16] using heat balance diagram to calibrate the model in place of detailed geometry. The model has been used to calculate the efficiency at different loads, blade angles assuming optimum turbine design conditions. The optimization of design parameters of a turbomachine flow behavior is critical and requires optimal dimensions of different components as well as airfoil shapes of rotor blades and nozzle [17]. The profile of the nozzle plays a vital role to minimize the huge amount of energy loss occurred due to flow separation. In this paper, the convergent type non-axisymmetric airfoil nozzle has been designed which can convert the pressure and thermal energy of the fluid into kinetic energy to obtain subsonic velocity and temperature drop at the outlet, which is essential for an effective design of turboexpander used in gas liquefaction applications. The design method is based on 3rd and

5th order curve fitting under specified boundary condition, which is suitable for the mean-line design and deliver uniform flow at the inlet of the turbine. This type of nozzle is essential for mixed-flow type turbine having radial inlet and an axial outlet. The rotor is of impulse type with a small amount of reaction. The expansion ratio in the nozzle is 2.85. For exact analysis point of view, experiments provided the exact results but it is expensive. Accurate prediction of flow field behavior, flow separation, pressure, velocity, Mach number, temperature, TKE etc. have been analyzed and compared among the BSL, k-ε, SST and SSG Reynolds stress turbulence model.

2. Mathematical Model

The oblique shocks occurred inside the nozzle can be minimized by obtaining the continuous contour profile of a nozzle. Due to this, the curve-fitting method has been used for the current application. The slope of the nozzle wall is continuously decreasing (convergent type) from inlet to the outlet of the nozzle. The geometrical specification of the nozzle is given in Table 1. After the outlet, the fluid is assumed to be tangent to the rotor. From the manufacturing point of view, the clearance of 1 mm has been taken in the present case (Fig. 1).

The nozzle is designed for a particular type of impulse turbine which is used in the liquefaction process of cryogenic fluids [18]. The impact of fluid is tangential to the turbine blade due to the airfoil design of nozzle which is shown in Fig. 1. The computational study of this type of nozzle is not available in open literature, so this work is done to fulfill this research gap.

2.1 Design of Lower Curve of the Nozzle

The lower curve of nozzle has been designed using third order (cubic) curve.

The cubic equation:

$$y = ax^3 + bx^2 + cx + d$$

Boundary conditions:

(1) $\frac{dy}{dx} = 0,\ at\ \ x = 0\ \ and\ \ y = 3$

(2) $\frac{dy}{dx} = 0,\ at\ \ x = 8.87\ \ and\ \ y = 0.90$

(3) $y = 0,\ at\ \ x = 0$

(4) $y = 0.90\ \ at\ \ x = 8.87$

2.2 Design of Upper Curve of the Nozzle

The upper curve of nozzle has been designed using fifth order curve is shown in equation.

The fifth order equation:

$$y = ax^5 + bx^4 + cx^3 + dx^2 + ex + f$$

Boundary conditions:

Table 1 Geometrical specification of the nozzle.

Geometrical Properties	Unit	Value
Pitch circle diameter	mm	38.500
Turbine wheel diameter	mm	25.000
Distance from inlet to tangent of wheel	mm	14.639
Nozzle width at outlet	mm	1.80
Height of the nozzle	mm	11.650
Clearance	mm	1.000
Axial distance from inlet to outlet	mm	8.8708
Nozzle angle (α) at inlet	Degree	18.686
Change of nozzle angle per unit length	Degree/mm	2.1836

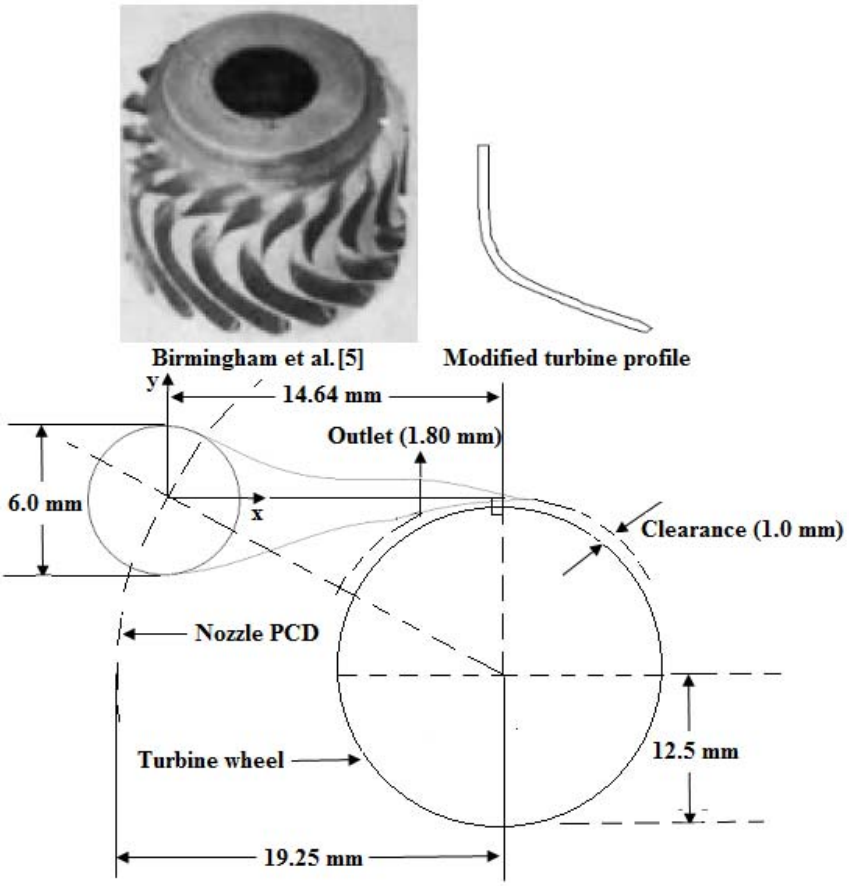

Fig. 1 Schematic diagram of nozzle and turbine wheel [18].

(1) $\frac{dy}{dx} = 0,\ at\ \ x = 0\ \ and\ \ y = 3$

(2) $y = 3,\ at\ \ x = 0$

(3) $y = 0.90\ \ at\ \ x = 8.87$

(4) $\frac{dy}{dx} = 0,\ at\ \ x = 8.87\ \ and\ \ y = 0.90$

(5) $\frac{dy}{dx} = 0,\ at\ \ x = 14.64\ \ and\ \ y = 0$

(6) $y = 0\ \ at\ \ x = 14.64$

A three-dimensional model has been developed based on the above equations and boundary conditions using Matlab© and Solidworks© which is shown in Fig. 2. The uniform thickness is given to the upper and lower curve (3.00 mm) to generate the upper and lower surfaces.

3. Numerical Method and Setup

The three-dimensional compressible Reynolds-averaged Navier-Stokes (RANS) equations with shear stress turbulence model with high-resolution advection scheme followed by finite volume method are used to solve the conservation of mass, momentum and energy equations by using the commercial CFD software ANSYS CFX©. Viscous work term has been taken into consideration while solving energy equation to predict the accurate heat transfer. There are several options available for turbulence models; out of which BSL, k-ε, SST and SSG Reynolds stress turbulence models have been used and results are compared.

- The following set-up has been used for above simulations:
- The high-resolution scheme has been used to discretize the advection terms.

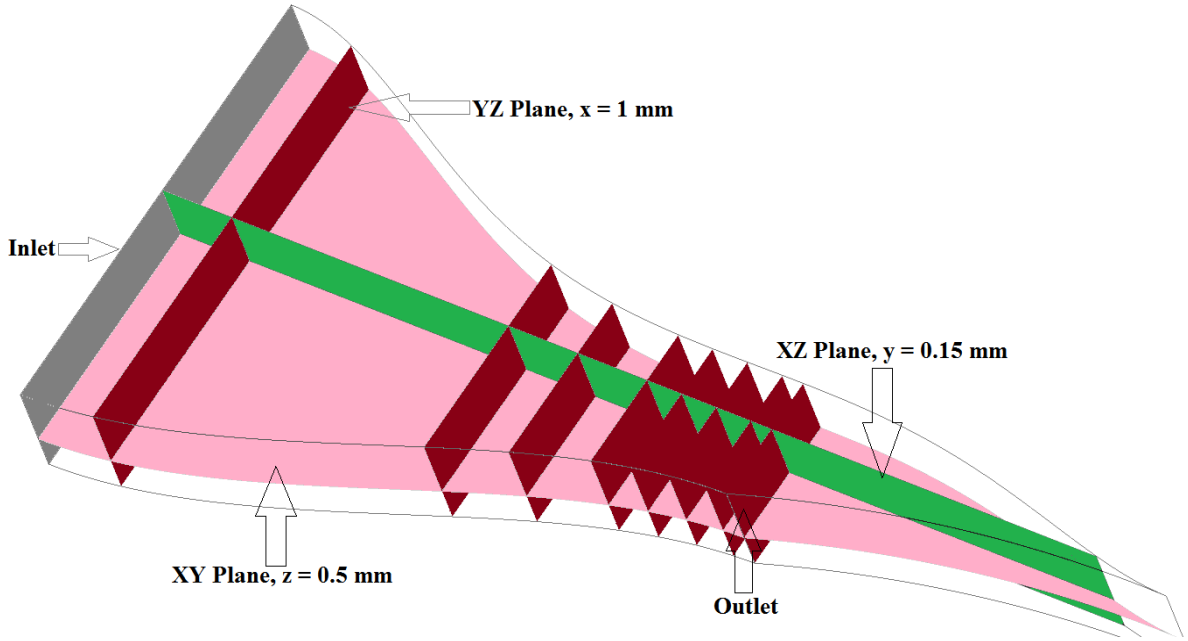

Fig. 2 Computational model of a non-axisymmetric convergent nozzle.

Table 3 Discretization schemes for different terms

	Advection scheme	Transient scheme
Continuity	Upwind	Second -order Backward Euler
Momentum	Upwind	Second -order Backward Euler
Energy	Upwind	Second -order Backward Euler
Turbulent kinetic energy	High-resolution	High-resolution
Turbulent eddy frequency	High-resolution	High-resolution

- The second order backward Euler discretization scheme is used for transient terms.
- Total energy option is used for transport of enthalpy with kinetic energy effects.
- The turbulent intensity of 5 % has been used.
- The computational domain is initialized by 10 pressure and 130 K temperature.
- No slip and adiabatic boundary condition are imposed on the wall.
- Air is used as a working fluid with Peng Robinson real gas assumption.

3.1 Turbulence Model and Discretization Scheme

The Shear-Stress Turbulence (SST) model is widely used due to it possesses combined advantages of k-ω near walls and k-ε in wakes and free-shear regions in the outer boundary layer. The SST model can also control the eddy-viscosity by restricting the turbulent shear stress, which improves the model performance in adverse pressure gradients and flows separation cases in particular. The governing equations, mass, momentum, and energy along with pressure based solver transient formulation are adopted in this case. To achieve the accurate simulation results, the selection of numerical scheme is equally important as turbulence model. Due to this reason, in the current study, the second-order upwind scheme is selected for discretization of momentum and energy equations and no-slip with adiabatic boundary condition is imposed on the wall as reported in Table 3. To increase the computational convergence, four aforementioned turbulence models are selected for RANS equations to predict the accurate numerical result. The SSG model provides better results as compared to the Launder, Reece & Rodi model for complex nonlinear structures [19]. The flow field structure is compared to these

models.

Governing equations

Continuity Equation:

$$\frac{\partial \rho}{\partial t} + \nabla.\left(\rho U\right) = 0$$

Momentum Equations:

$$\frac{\partial \left(\rho U\right)}{\partial t} + \nabla.\left(\rho U \otimes U\right) = -\nabla p + \nabla.\tau + S_M$$

Where S_M is the sum of body forces and τ is the stress tensor which is related to the strain rate as:

$$\tau = \mu\left(\nabla U + \left(\nabla U\right)^T - \frac{2}{3}\delta\nabla.U\right)$$

Total Energy Equation:

$$\frac{\partial \left(\rho h_{tot}\right)}{\partial t} - \frac{\partial p}{\partial t} + \nabla.\left(\rho U h_{tot}\right) = \nabla.\left(\lambda\nabla T\right) + \nabla.\left(U.\tau\right) + U.S_M + S_E$$

Where h_{tot} is the total enthalpy which is related to static enthalpy:

$$h_{tot} = h + \frac{1}{2}U^2$$

Real gas equation Peng Robinson model:

$$p = \frac{RT}{v-b} - \frac{a\left(T\right)}{v^2 + 2bv - b^2}$$

where:

$$b = 0.0778\frac{RT_c}{P_c}$$

$$a\left(T\right) = a_0\left(1 + n\left(1 - \sqrt{\frac{T}{T_c}}\right)\right)^2$$

$$a_0 = 0.45724\frac{R^2T_c^2}{P_c}$$

and 'n' is calculated as follows:

$$n = 0.480 + 1.574?- 0.176\omega^2$$

3.2 Solution Approach and Boundary Condition

In the current paper, the flow field characteristic of a convergent nozzle is reported. The second order implicit scheme is used for the advancement of the solution with a specified linear solver.

Finite volume method is used to discretize the domain and solved the Reynolds averaged Navier-Stokes (RANS) equation. The transient method with advection scheme and upwind discretization method has been used to discretize the domain whereas second order backward Euler upwind scheme is used for solver control. The convergence criteria (RMS) and convergence target are set to be 10^{-6} and 0.001 respectively. Total energy with BSL, k-ε, SST and SSG Reynolds stress turbulence model including viscous work term is used to solve the fluid domain. For dynamic model control, automatic pressure level information, temperature damping, and velocity pressure coupling with Rhie-Chow fourth order model is used. The real gas equation Peng Robinson has also been used. The following set-up has been used for this simulation:

- Inlet: Total pressure (10 bar) and total temperature (130 K) at the inlet of the nozzle and the fluid flows normal to the inlet.
- Outlet: Subsonic outflow condition with an average pressure of 3.5 bar and pressure blend of 0.05.
- Wall: No slip and adiabatic boundary condition are imposed on the wall.
- Initialization: The inlet pressure and temperature have been used.

For computation, an unstructured grid with tetrahedral cells with prim layers is used. In addition, a fine grid has been used near the wall of the nozzle and the grid becomes coarser as one moves away from the wall. The numerical simulations are conducted using Intel®Xeon®CPU E5-1660 v3 @ 3.00 GHz with 64 GB RAM memory.

3.3 Grid Independency Test

To the best of the author's knowledge, there is no study available in the open literature about the non-axisymmetric convergent airfoil nozzle. In order

to compute the flow field inside the nozzle, a grid independent analysis is carried out with the three different mesh resolutions: 168924 (Coarse), 198609 (medium) and 270494 (fine).

Fig. 3 shows the velocity variation along the axial distance. It may be noted that all sets show the similar trend, but a more converged solution is obtained with 270494. Further refinement is not realistic due to very small change in results but takes more computational times. Therefore, a grid resolution of 270494 is selected for the remainder of the simulations for all the models, as shown in Fig. 4.

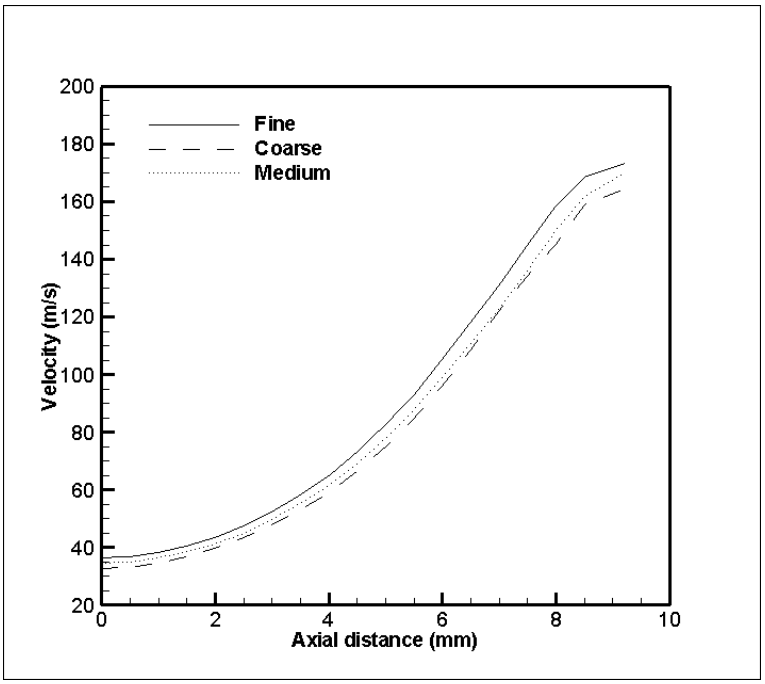

Fig. 3 Variation of velocity for different grid resolutions.

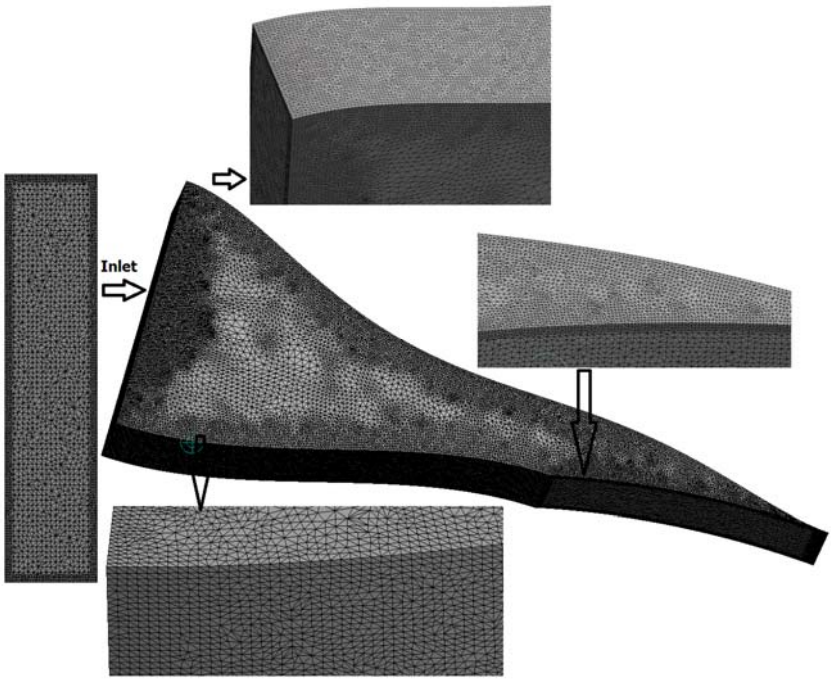

Fig. 4 Configuration of 3D cells at different locations.

4. Results and Discussion

An exhaustive study is carried out to study the fluid flow behavior (air) inside the non-axisymmetric convergent nozzle. The flow characteristics are presented as contours of velocity, Mach number, eddy viscosity, while thermal properties are presented in the form of contours of temperature, static enthalpy and static entropy at the cost of pressure drop. The real fluid flow inside the nozzle will be certainly of three-dimensional in nature. Four turbulence models (BSL, k-ε, SSG, and SST) are applied to obtain the fluid flow characteristics inside the nozzle. The flow fields in the Y-Z, X-Y and X-Z planes along the axial distance (inlet to outlet) are reported.

Fig. 5 shows the contours of pressure distribution at different cross-sections.

It is clearly observed that the variation of pressure for air is from 10.00 bar at the inlet to 3.50 bar at the outlet (Pressure ratio of 2.85) which is the desirable condition of the fluid at the turbine inlet. From the aforementioned pressure contours, it is observed that pressure does not change significantly up to the axial distance of x=2.50 mm due to the relatively lesser slope of the curve. The drop in pressure is higher in between the axial distance of x=2.5 mm to x=6 mm thereafter sudden contraction in slope is occurred due to which pressure decreases at a higher rate to achieve the desirable Mach number at the inlet of the turbine. In this process, a considerable amount of temperature is reduced due to enthalpy drop which is shown in Fig. 6. It is interesting to note that the pressure drop for all the models isapproximately similar.

Fig. 7(a-d) represents the velocity contours of air at various planes inside the nozzle for different models.

It is shown in the figure that the velocity of air at plane x = 2.50 mm is approximately 47.47, 46.74, 47.65 and 47.17 m/s for respectively due to small change in pressure thereafter it continuously increases as one moves towards the outlet where it is approximately 180.90, 176.57, 184.76 and 178.72 m/s with Mach number of 0.85, 0.82, 0.86 and 0.83 respectively as shown in Fig. 8.

The main reason for the increase in velocity is due to drop in pressure. It is interesting to observe that Mach number at the outlet of the nozzle is highest for SSG model which is desirable for the aforementioned impulse turbine used in a turboexpander. The velocity streamline shows that there is no flow separation or vortex formation occurs inside the nozzle, which reduces the losses inside the nozzle and increases the efficiency of the system. Fig. 9 shows the streamline for all the models. The flow separation can be seen at the upper wall in the vicinity of the inlet thereafter the flow becomes fully developed. There is no vortex formation inside the domain due to which the losses are minimized.

Fig. 10 (a-d) represents the temperature contour from the inlet to the outlet at different cross-sections. It shows that the temperature of the air at the outlet of the nozzle is 114.44, 115.27, 113.90 and 114.82 K for BSL, k-ε, SSG, and SST model respectively, which shows the decrease in temperature of 15.56, 14.73, 16.1 and 15.18 K respectively. The decrease in temperature inside the nozzle is very much important.

It is observed that the decrease in temperature for SSG and k-ε model is highest and lowest respectively. The other two models i.e. BSL and SST have almost similar temperature and velocity variations. The temperature drop is directly related to the variation of static enthalpy and entropy of air which is shown in Fig. 11. The entropy generation for SSG model is minimum which is the reason for the highest drop in temperature as compared to the other models. This decrease in temperature is very much important at ultra-low temperature because it happens inside the nozzle, which reduces the turbine work and hence increases the efficiency of turboexpander. It is desirable for the liquefaction of gases.

Fig. 12 represents the variation of density along the axial distance. It shows approximately similar density

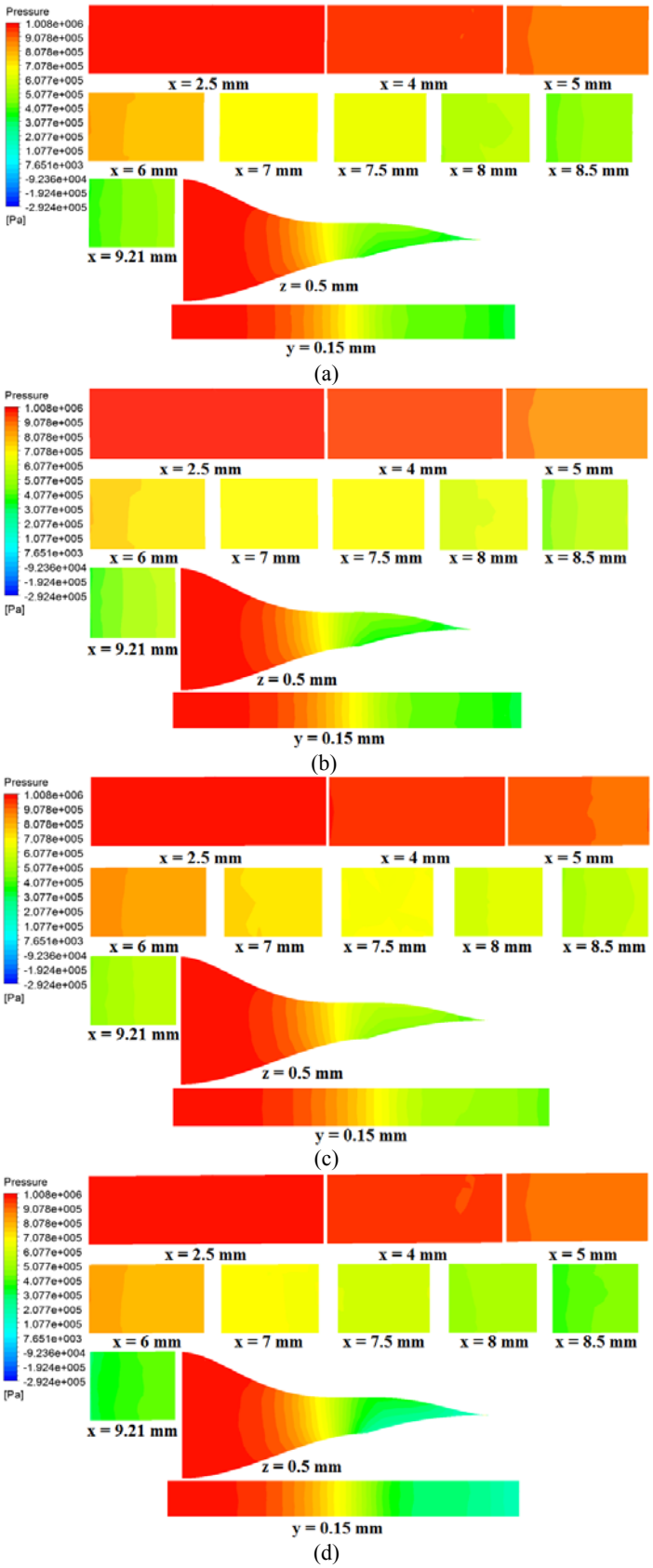

Fig. 5 Pressure contours at different cross-sections: (a) BSL; (b) K-epsilon; (c) SSG; (d) SST.

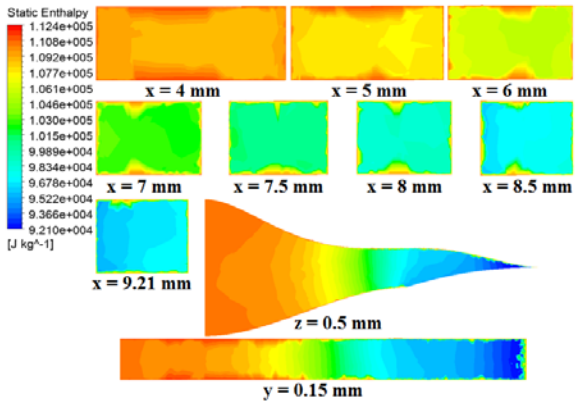

(a)

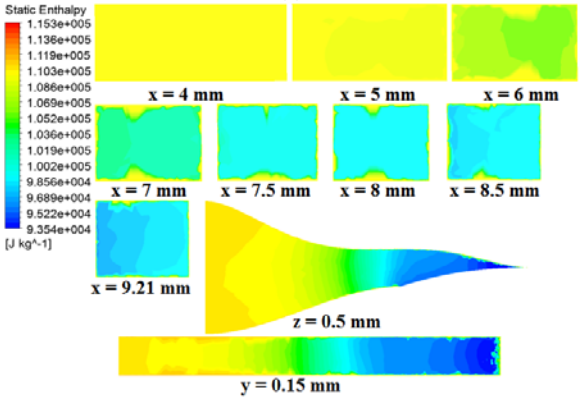

(b)

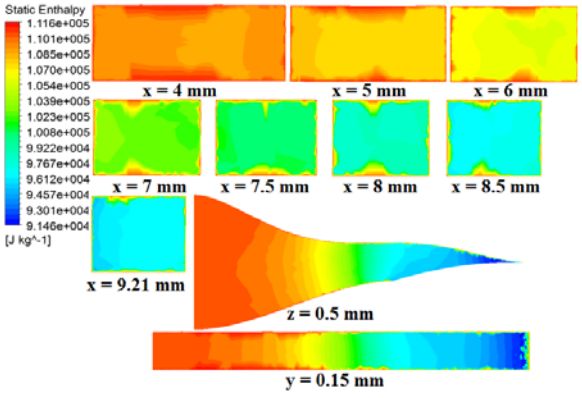

(c)

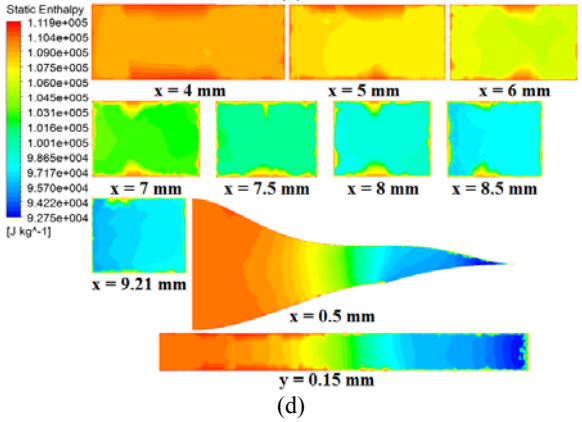

(d)

Fig. 6 Static enthalpy contours at different cross-sections: (a) BSL; (b) K-epsilon; (c) SSG; (d) SST.

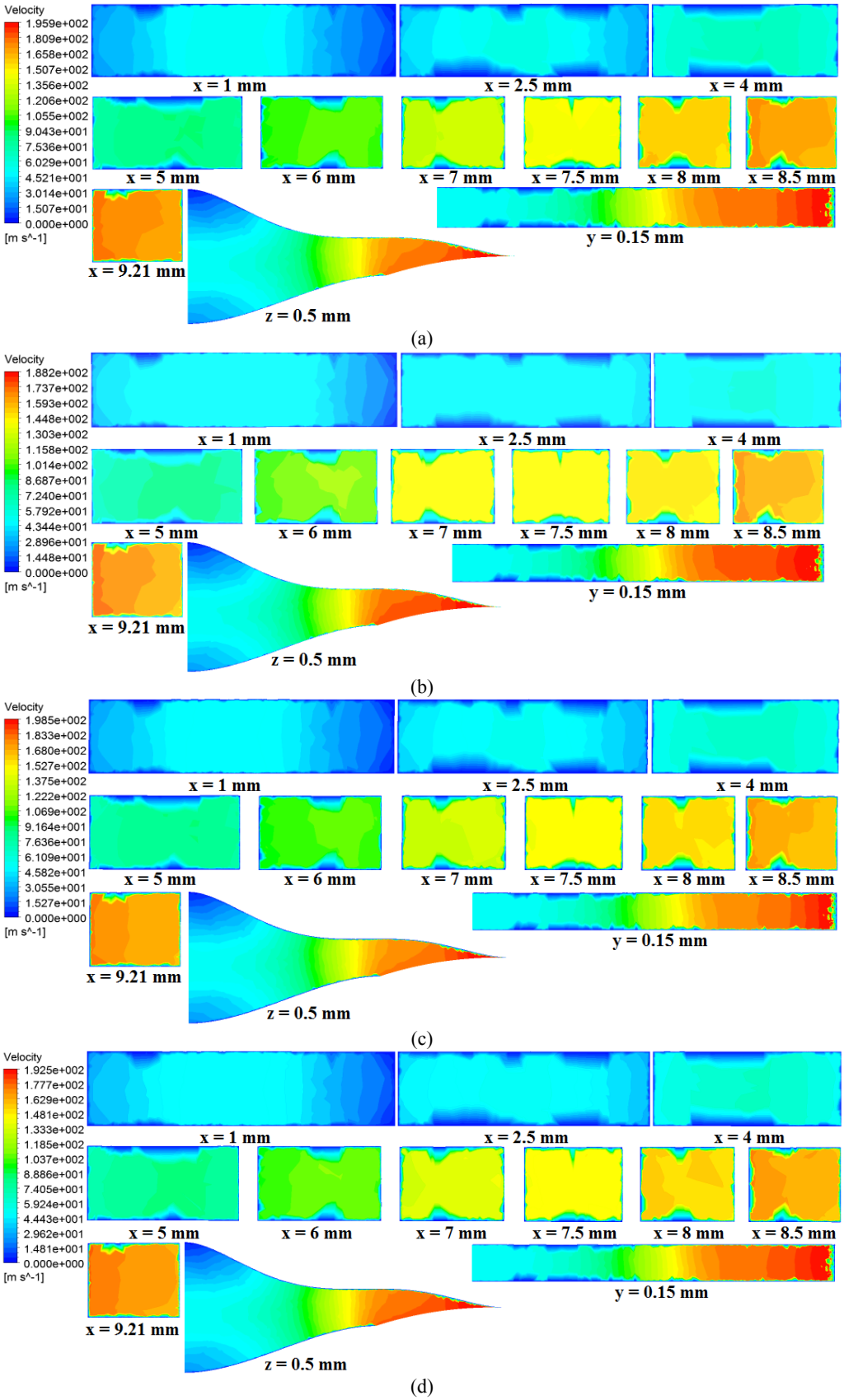

Fig. 7 Velocity contours at different cross-sections: (a) BSL; (b) K-epsilon; (c) SSG; (d) SST.

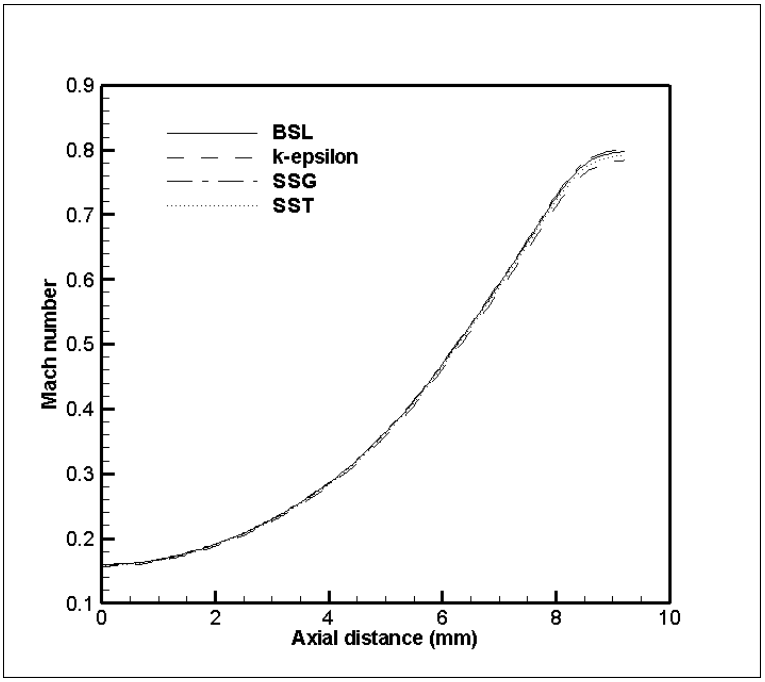

Fig. 8 Mach number distribution from inlet to outlet.

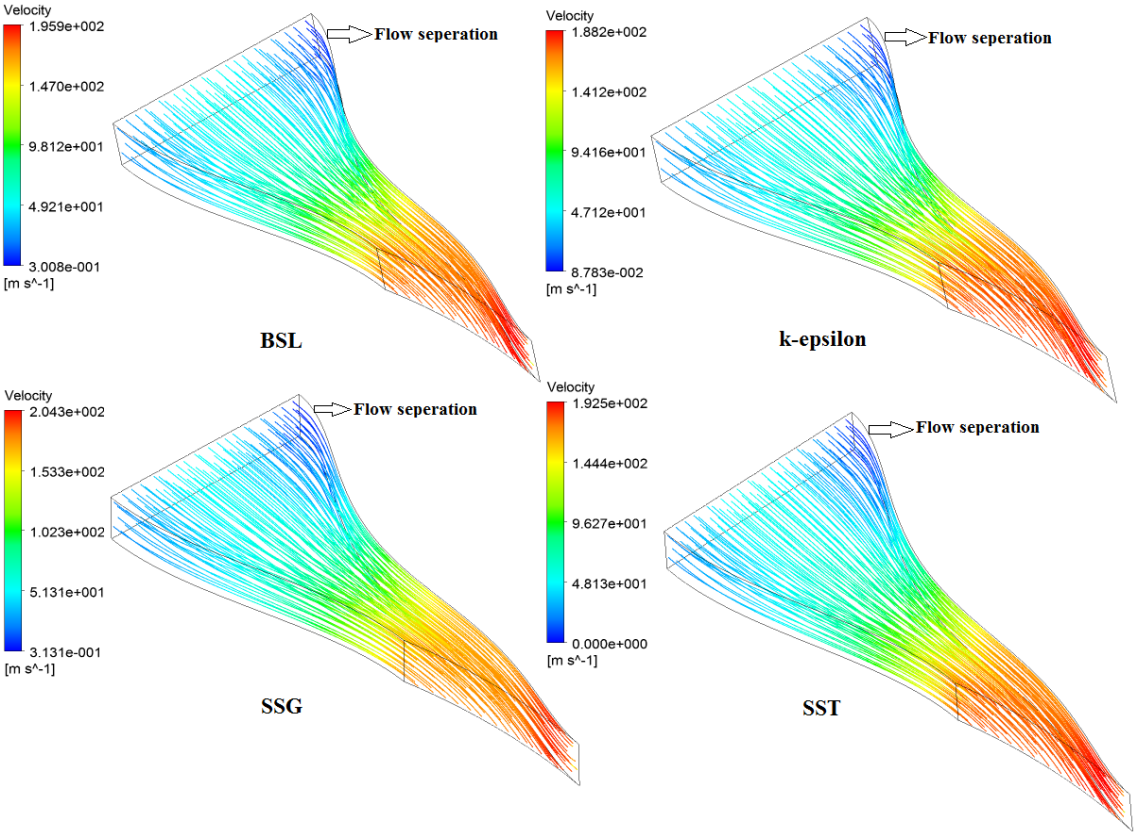

Fig. 9 Velocity streamlines for different models.

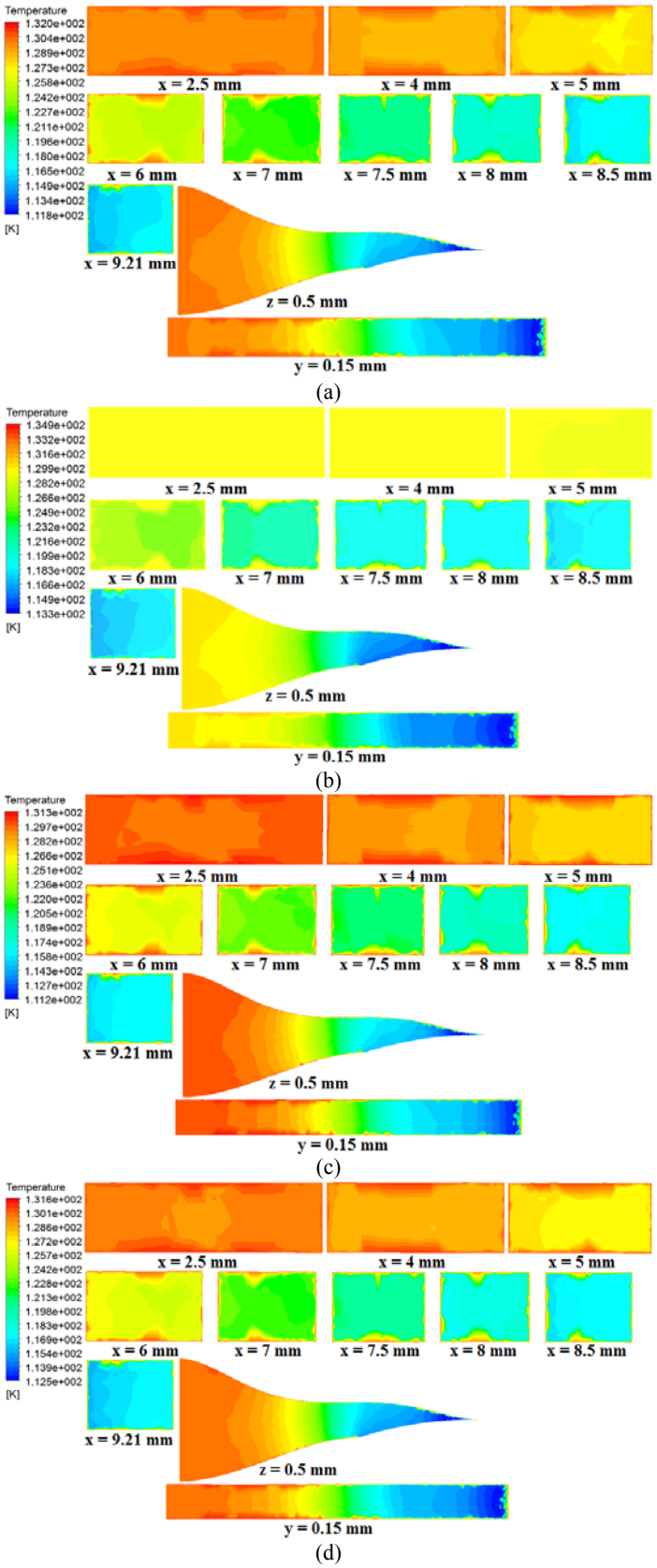

Fig. 10 Temperature contours at different cross-sections: (a) BSL; (b) K-epsilon; (c) SSG; (d) SST.

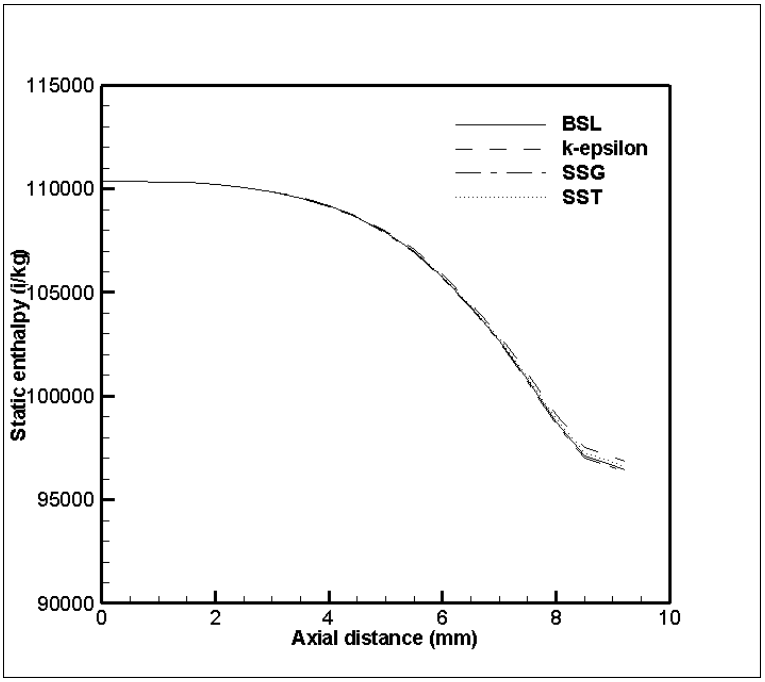

(a)

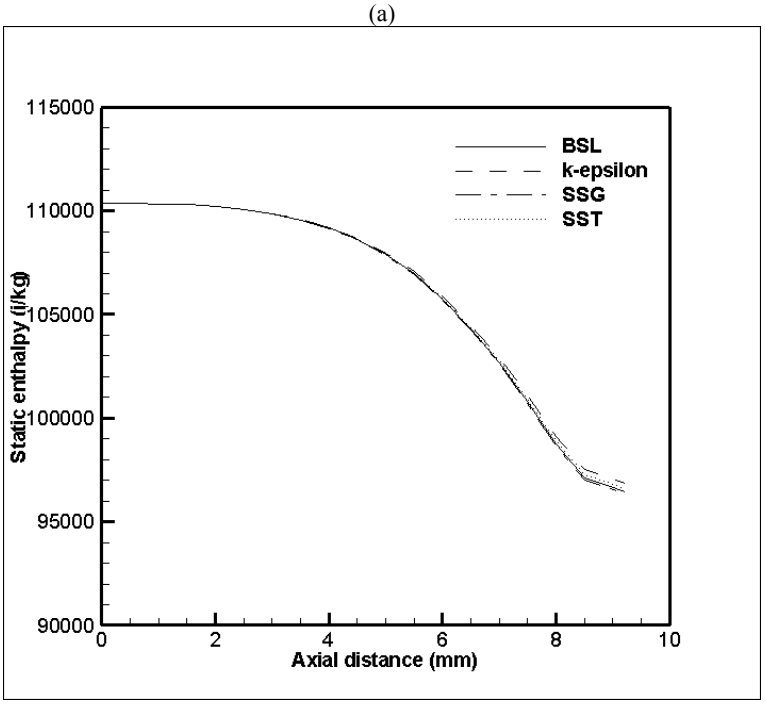

(b)

Fig. 11 (a) Static enthalpy; (b) entropy variation along the axial distance.

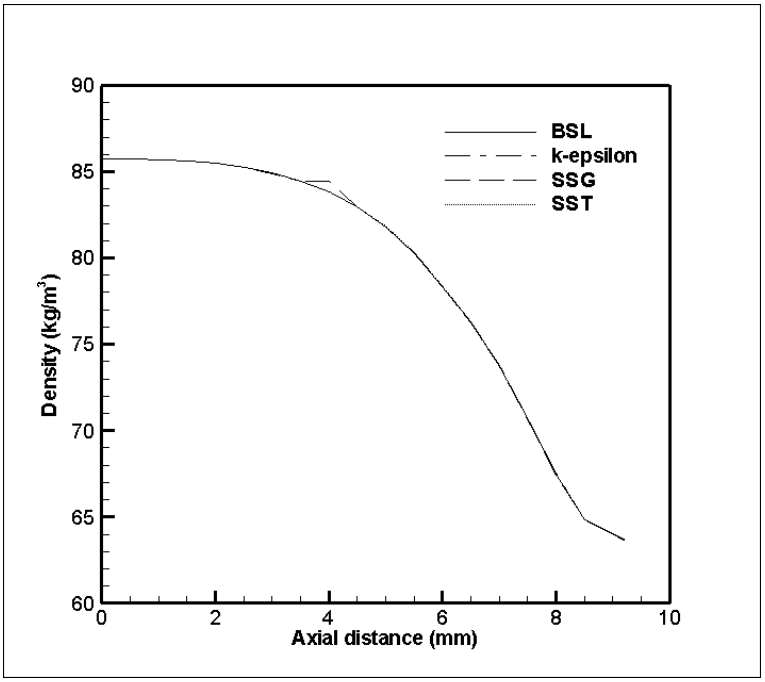

Fig. 12 Density variation along the axial distance.

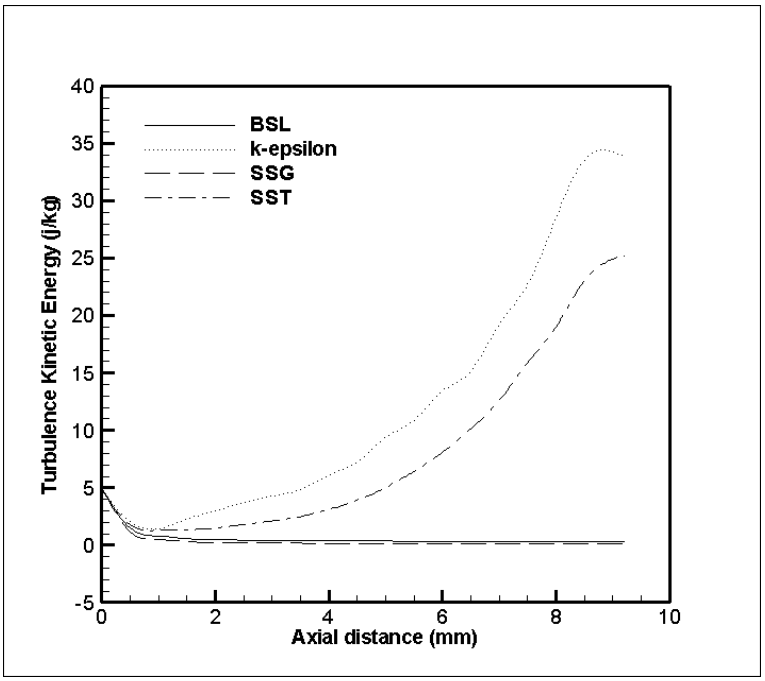

Fig. 13 Turbulent kinetic energy along the axial distance.

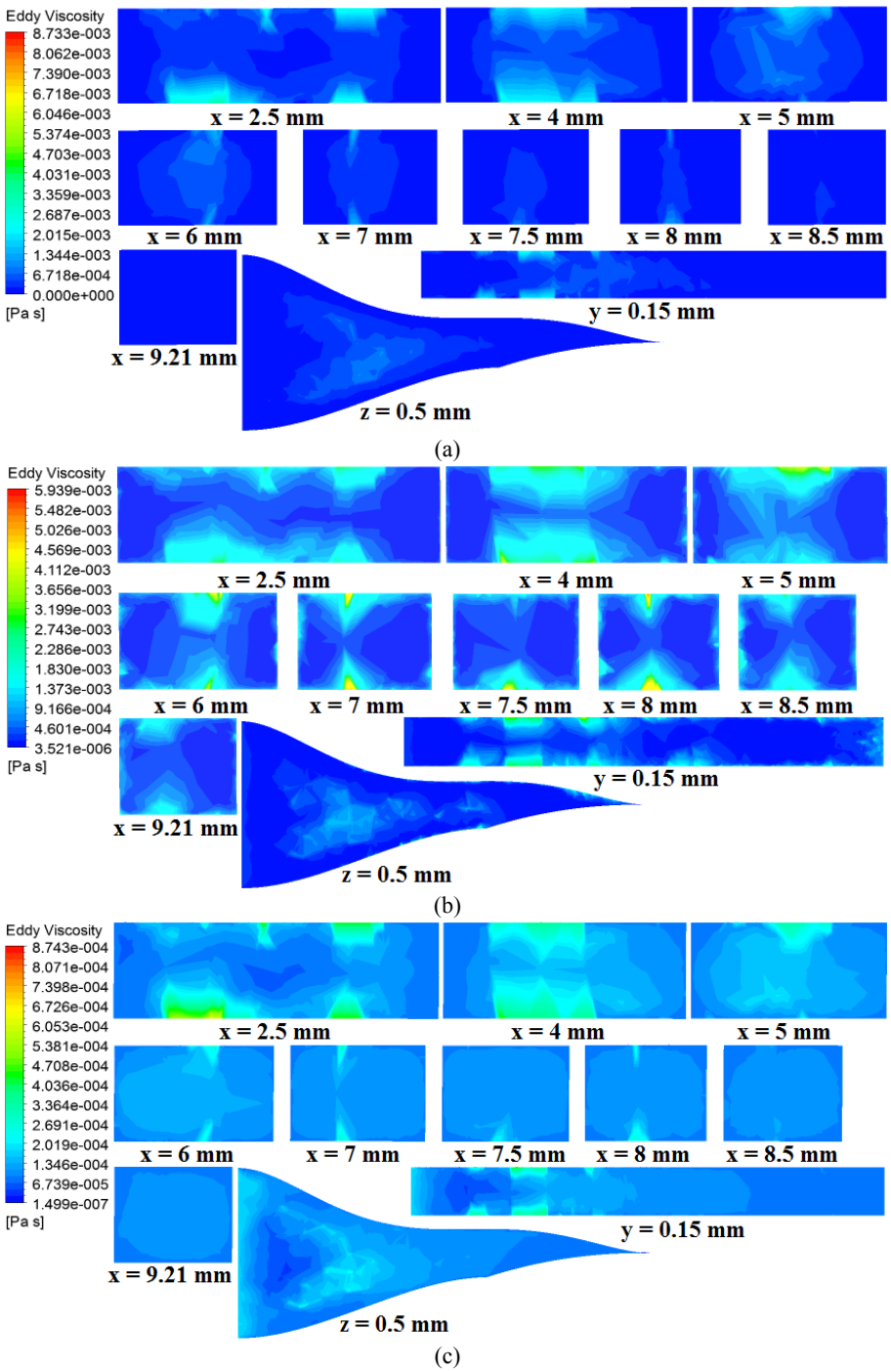

Fig. 14 Eddy viscosity contours at at different cross-sections (a) BSL; (b) K-epsilon; (c) SSG; (d) SST.

variation from inlet to outlet. The density at the inlet is 85.73 kg/m^3 and that is at the outlet is 59.65 kg/m^3 for all the models only exception is a k-ε model for which it is 58.96 kg/m^3 . It indicates that the density reducing after x=3.50 mm at a relatively higher rate due to increase in convergent slope of the nozzle.

In turbulent flow, the TKE is measured for the development or decrease in turbulence. Fig. 13 represents the variation of turbulent kinetic energy (TKE) along the axial distance. It shows that up to x = 1.00 mm, the trend of TKE for all the models are similar thereafter it is highest for k-ε model whereas it

is minimum and approximately similar to BSL and SSG model. It is also used to visualize the flow effects in eddy viscosity. Although, it is not a property of fluid rather it is significantly affected by the fluid flow characteristics, the shape of the computational domain and free stream turbulence intensity. SST model overestimates the turbulence in flow regime due to which the eddy viscosity shows the degree of strength of eddy diffusion and its distribution.

Fig. 14 represents the variation of eddy viscosity at various planes. It is noticed that the eddy viscosity effects at lower and upper wall up to x=4.00 mm for all the models thereafter, its intensity increases at the sidewalls also except BSL model whereas the pattern is similar for k-ε and SST model after x=7.00 mm but the value is greater for the SST model. It also shows that it is completely obsolete for BSL model and minimum for SSG model. For all the cases, the intensity of eddy viscosity is reduced as one moves towards the outlet which is desirable to reduce the turbulence losses inside the nozzle. at x=7.5 and 8.00 mm, the intensity of eddy viscosity is maximum at the bottom and top wall for k-ε and SST model.

5. Conclusion

The current work proposes a novel design methodology using curve-fitting approach for the geometry of non-axisymmetric convergent nozzle and validation of the methodology based on computational approach. The numerical simulation is carried out to visualize the fluid flow behavior such as velocity, pressure, Mach number, density, eddy viscosity and TKE. The analysis is extended to study the thermal behaviors such as temperature, static enthalpy, and entropy at various cross-sections. The turbulence models such as BSL, k-ε, SSG, and SST is used for to predict the fluid flow at a pressure ratio of 2.85. The SSG model for the current application shows a maximum drop in temperature and highest Mach number in the order of 16.1 K and 0.86 respectively. The maximum drop in temperature is because of lowest entropy generation. From this study, it is concluded that the curve fitting method and SSG model for numerical simulations are an efficient tool to design and predict the flow pattern inside the nozzle. The author believes, the simplified methodology for designing nozzle will be helpful for the researchers, working on cryogenic turboexpander for the liquefaction of gases.

References

[1] Ohira, K., Nakayama, T., and Nagai, T. 2012." Cavitation flow Instability of Subcooled Liquid Nitrogen in Converging-Diverging Nozzles." *Cryogenics* 52: 35-44. DOI: 10.1016/j.cryogenics.2011.11.001.

[2] Dadone, A., and Grossman, B. 2003. "Fast Convergence of Inviscid fluid Dynamic Design Problems." *Computers & Fluids* 32: 607-27.

[3] Scalabrin, L. C., and Azevedo, J. L. F. 2004. "Adaptive Mesh Refinement and Coarsening for Aerodynamic Flow Simulations." *International Journal for Numerical Methods in Fluids* 45 (10): 1107-22.

[4] Tsui, Y. Y., and Wu, T. C. 2009. "Use of Characteristic-Based Flux Limiters in a Pressure-Based Unstructured-Grid Algorithm Incorporating High-Resolution Schemes." *Numerical Heat Transfer, Part B: Fundamentals* 55 (1): 14-34.

[5] Horisawa, H., Sawada, F., Onodera, K., and Funaki, I. 2008. "Numerical Simulation of Micro-nozzle and Micro-nozzle-array Flowfield characteristics." *Vacuum* 83 (1): 52-6.

[6] Hasan, A. T. 2014. "Characteristics of Overexpanded Nozzle Flows in Imposed Oscillating Condition." *International Journal of Heat and Fluid Flow* 46: 70-83.

[7] Mousavi, S. M., and Roohi, E. 2014. "Three Dimensional Investigation of the Shock Train Structure in a Convergent–Divergent Nozzle." *Acta Astronautica* 105 (1): 117-27.

[8] Von Lavante, E., Kaya, H., Winzösch, F., Brinkhorst, S., and Mickan, B. 2015. "Flow Structure in Critical Flow Venturi Nozzle and Its Effect on the Flow Rate." *Flow Measurement and Instrumentation* 44: 97-106.

[9] Chen, P., Wu, F., Xu, J., Feng, X., and Yang, Q. 2016. "Design and Implementation of Rigid-Flexible Coupling for a Half-Flexible Single Jack Nozzle." *Chinese Journal of Aeronautics* 29 (6): 1477-83.

[10] Chung, H., Hong, C. W., Kim, S. H., Cho, H. H., and Moon, H. K. 2016. "Heat Transfer Measurement near Endwall Region of First Stage Gas Turbine Nozzle Having Platform Misalignment at Combustor-Turbine

Interface." *International Communications in Heat and Mass Transfer* 78: 101-11.

[11] Chaudhuri, A., and Hadjadj, A. 2016. "Numerical Investigations of Transient Nozzle Flow Separation." *Aerospace Science and Technology* 53: 10-21.

[12] Quaatz, J. F., Giglmaier, M., Hickel, S., and Adams, N. A. 2014. "Large-Eddy Simulation of a Pseudo-Shock System in a LAVAL Nozzle." *International Journal of Heat and Fluid Flow* 49: 108-15.

[13] Kamali, R., Mousavi, S. M., and Binesh, A. R. 2015. "Three Dimensional CFD Investigation of Shock Train Structure in a Supersonic Nozzle." *Acta Astronautica* 116: 56-67.

[14] Afroosheh, M., Vakilimoghaddam, F., and Paraschivoiu, M. 2017. "Boundary Layer Effects on the Critical Nozzle of Hydrogen Sonic Jet." *International Journal of Hydrogen Energy* 42 (11): 7440-6.

[15] Turgut, Ö. H., and Camci, C. 2016. "Factors Influencing Computational Predictability of Aerodynamic Losses in a Turbine Nozzle Guide Vane Flow." *Journal of Fluids Engineering* 138 (5): 051103.

[16] Fuls, W. F. 2017. "Accurate Stage-by-Stage Modelling of Axial Turbines Using an Appropriate Nozzle Analogy with Minimal Geometric Data." *Applied Thermal Engineering* 116: 134-46.

[17] Kler, A., and Zakharov, Y. 2017. "Joint Optimization of Power Plant Cycle Parameters and Gas Turbine Flow Path Parameters with Blade Airfoils Represented by Cubic Splines." *Energy* 137: 183-92.

[18] Birmingham, B. W., Sixsmith, H., and Wilson, W. A. 1962. "The Application of Gas-Lubricated Bearings to a Miniature Helium Expansion Turbine." In *Advances in Cryogenic Engineering* (pp. 30-42). Springer, Boston, MA.

[19] Speziale, C. G., Sarkar, S., and Gatski, T. B. 1991. "Modelling the Pressure-Strain Correlation of Turbulence: An Invariant Dynamical Systems Approach." *Journal of Fluid Mechanics* 227: 245-72.